THE JOURNAL OF PHYSICAL CHEMISTRY B

Article

pubs.acs.org/JPCB

Coulomb Repulsion in Short Polypeptides

Amir Norouzy, Khaleel I. Assaf, Shuai Zhang, Maik H. Jacob,* and Werner M. Nau*

Department of Life Sciences and Chemistry, Jacobs University Bremen, Campus Ring 1, D-28759 Bremen, Germany

Supporting Information

ABSTRACT: Coulomb repulsion between like-charged side chains is presently viewed as a major force that impacts the biological activity of intrinsically disordered polypeptides (IDPs) by determining their spatial dimensions. We investigated short synthetic models of IDPs, purely composed of ionizable amino acid residues and therefore expected to display an extreme structural and dynamic response to pH variation. Two synergistic, custom-made, time-resolved fluorescence methods were applied in tandem to study the structure and dynamics of the acidic and basic hexapeptides Asp_6, Glu_6, Arg_6, Lys_6, and His_6 between pH 1 and 12. (i) End-to-end distances were obtained from the short-distance Förster resonance energy transfer (sdFRET) from N-terminal 5-fluoro-L-tryptophan (FTrp) to C-terminal Dbo. (ii) End-to-end collision rates were obtained for the same peptides from the collision-induced fluorescence quenching (CIFQ) of Dbo by FTrp. Unexpectedly, the very high increase of charge density at elevated pH had no dynamical or conformational consequence in the anionic chains, neither in the absence nor in the presence of salt, in conflict with the common view and in partial conflict with accompanying molecular dynamics simulations. In contrast, the cationic peptides responded to ionization but with surprising patterns that mirrored the rich individual characteristics of each side chain type. The contrasting results had to be interpreted, by considering salt screening experiments, N-terminal acetylation, and simulations, in terms of an interplay of local dielectric constant and peptide-length dependent side chain charge−charge repulsion, side chain functional group solvation, N-terminal and side chain charge−charge repulsion, and side chain−side chain as well as side chain−backbone interactions. The common picture that emerged is that Coulomb repulsion between water-solvated side chains is efficiently quenched in short peptides as long as side chains are not in direct contact with each other or the main chain.

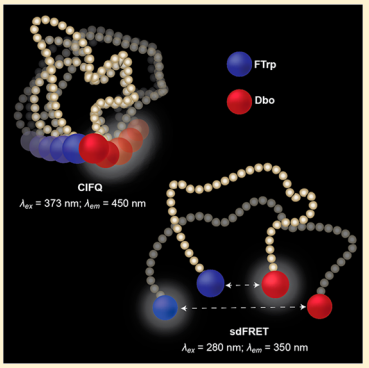

INTRODUCTION

Electrostatic repulsion between like-charged side chains is considered to determine the dimensions of natively unfolded or intrinsically disordered peptides and proteins (IDPs), and to influence their biological function.[1−7] For instance, the radius of gyration of protamine peptides, cationic IDPs rich in arginine, correlates with the positive net charge per residue.[1] The radius of gyration of human prothymosin α, an acidic IDP rich in aspartate and glutamate and with a net charge per residue of minus 0.4, is effectively reduced from ∼40 to ∼30 Å, when the charges are screened in the presence of 1 M KCl.[2] Repulsive Coulomb forces can also control chain dimensions during the refolding of regular proteins.[8,9] These new prospective insights encourage systematic studies on how Coulomb repulsion affects the unstructured polypeptide chain. Particularly, the short chain should be understood before any simulation-based prediction on the behavior of the long chain can be trusted. However, as the reservoir of biophysical methods to study the structure and dynamics of short polypeptides is limited, investigations on short chains have remained scarce.

We have previously developed two time-resolved fluorescence methods tailored to investigate polypeptide chains between 2 and 22 residues.[10−18] Here, we demonstrate that, when used in tandem, the methods provide synergistic information on chain structure and dynamics. The methods are based on the two unique photophysical properties of 2,3-diazabicyclo[2.2.2]oct-2-ene (DBO) incorporated into peptides as asparagine derivative Dbo (Figure 1).[16] DBO has the longest fluorescence lifetime among organic fluorophores, 325 ns in aerated water.[18] Yet, its fluorescence is effectively quenched upon collision with tryptophan (Trp) or with the equally effective Trp derivative 5-fluoro-L-tryptophan (FTrp, Figure 1), which we have chosen for this work, because of its advantageous photophysical characteristics.[19,20] When FTrp and Dbo are appended to the termini of a polypeptide, they can rapidly diffuse and collide during the long fluorescence lifetime of Dbo. The frequency of end-to-end collision, the collision rate, is then easily obtained by comparing the Dbo lifetimes in the presence and absence of FTrp (Figure 2).[17] This rate provides a direct measure of chain end-to-end flexibility, and depends on the equilibrium distance distribution and intrachain diffusion but also, as emphasized in this work, on local interaction forces when probe-labeled regions come close.[17,18] The second unique property of DBO is its small oscillator strength with an extinction coefficient of only 50 M^{-1} cm^{-1} at 350 nm in water. The DBO absorption spectrum and the FTrp fluorescence spectrum extend over the same range of

Received: August 15, 2014
Revised: November 6, 2014
Published: December 3, 2014

   dx.doi.org/10.1021/jp508263a | J. Phys. Chem. B 2015, 119, 33−43

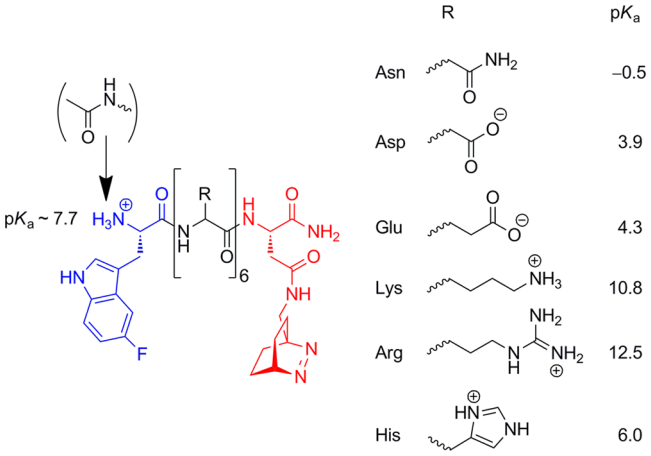

Figure 1. Chemical structures of the N- and C-terminally conjugated fluorophores, 5-fluoro-L-tryptophan (FTrp, blue), 2,3-diazabicyclo[2.2.2]oct-2-ene (DBO), and DBO-labeled amidated asparagine (Dbo, red) in acidic (Glu, Asp) and basic (Lys, Arg, His) peptides.

wavelengths such that optically excited FTrp can be deactivated by Förster resonance energy transfer (FRET) to DBO that now acts as energy acceptor (Figure 2). The small DBO extinction coefficient is responsible for the short critical radius (R_0 ca. 10 Å), which ensures that energy transfer becomes effective only at distances below 20 Å and that an effective distance can be diagnosed with an unprecedented sub-Ångstrom resolution. As we previously discussed in detail,[10−14] the effective distance depends not only on the equilibrium distance distribution but also on intrachain diffusion. In contrast to the collision rate, however, it should show little sensitivity to local repulsive interactions between probe-labeled chain regions.

We will refer to the first method as collision-induced fluorescence quenching (CIFQ) and to the second as short-distance FRET (sdFRET). To switch from one method to the other merely requires adjustment of the excitation wavelength (Figure 2). We have already used CIFQ to establish a flexibility scale for the side chains of natural amino acids in peptides.[17] This scale depended strongly on side chain type and bulk and apparently less on side chain charge status, but already these preliminary experiments pointed to the question of Coulomb-force influence. In a follow-up study, we analyzed the β-sheet and found its β-turn segments to be considerably more flexible than its β-strand segments, while substitution of charged side chains did not measurably alter segment flexibility.[21] Therefore, we ask here for the impact of repulsion in sequences with six ionizable residues in a row: Such homorepeat peptides have important biological functions[22] and warrant a maximal variation of charge status when the solution pH is varied from 1 to 12. In the acidic hexapeptides, Asp_6 and Glu_6, electrostatic repulsion is "switched on" upon deprotonation and was expected to stretch the chains. In the basic chains, His_6, Arg_6, and Lys_6, Coulomb repulsion is "switched off" upon deprotonation and was expected to be accompanied by profound contraction. MD simulations are already trusted to give insight into the behavior of long chains, of the refolding protein,[23] and proved also here to be invaluable in the interpretation of the experiments.

RESULTS

Design of Peptide Sequences. A peptide chain composed of nonionizable residues should display no pH-induced dynamical or structural response. Coulomb effects could vary only when the charge status of the free N-terminal amino group and C-terminal carboxylate group is altered. We therefore used, with one exception, peptides with an amidated, neutral C-terminus. We further included chains with an acetylated, neutral N-terminus in our study to pinpoint potential charge interactions inflicted by the N-terminus. The different types of chains are surveyed in Table 1, where we also introduce a convenient short notation and list the single-labeled reference peptides that the CIFQ or sdFRET analyses require when utmost precision is the goal.

Absence of pH Effects in Peptides with Nonionizable Side Chains (Asparagine). As an initial negative control experiment, and as a general test of whether the CIFQ/sdFRET method tandem is suited for the investigation of pH-induced Coulomb effects, we performed the required sets of experiments (double-labeled peptide and the two single-labeled reference peptides) on Asn_6. Because its side chains were neutral, and because the C-terminus was amidated, no change of attractive or repulsive Coulomb effects was expected over the pH range from 1 to 12. Indeed, in CIFQ measurements, the fluorescence kinetic traces of the double-labeled Asn_6 peptide measured between pH 1 and 12 coincided, as did the kinetic traces of the reference peptide (Figure 3a). The collision rate constant, k_q, was determined from the amplitude-weighted fluorescence lifetime of the double-labeled peptide (τ_D) and of the single-labeled reference peptide (τ_S) by using the equation

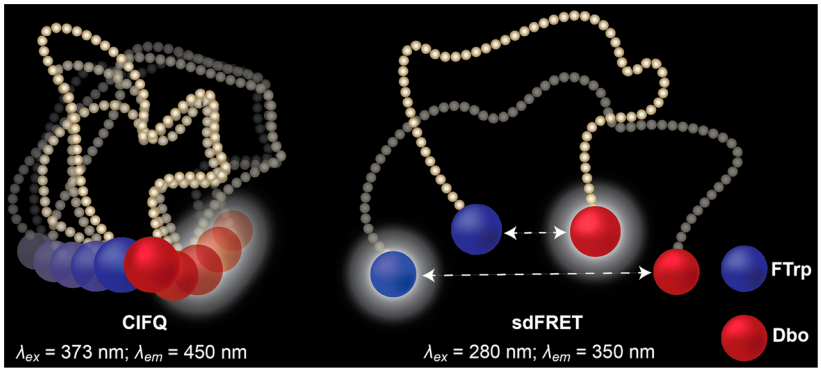

Figure 2. CIFQ: Following excitation of Dbo, quenching by FTrp occurs upon collision. sdFRET: Following excitation of FTrp, energy transfer to Dbo occurs at distances between 5 and 20 Å.

dx.doi.org/10.1021/jp508263a | J. Phys. Chem. B 2015, 119, 33−43

Table 1. Experimentally Investigated Peptide Sequences and Terminal Protection Groups

peptide [short notation][a]	reference for CIFQ[b] [short notation]	reference for sdFRET[c] [short notation]
Peptides with Amidated C-Terminus (Only N-Terminal Charges Possible)		
H_2N-FTrp-Xaa_6-Dbo-$CONH_2$	H_2N-Xaa_6-Dbo-$CONH_2$	H_2N-FTrp-Xaa_6-$CONH_2$
[Xaa_6]	[Xaa_6-Dbo]	[FTrp-Xaa_6]
Peptides with Amidated C-Terminus and Acetylated N-Terminus (No Terminal Charges Possible)		
AcNH-FTrp-Xaa_6-Dbo-$CONH_2$	AcNH-Xaa_6-Dbo-$CONH_2$	AcNH-FTrp-Xaa_6-$CONH_2$
[Ac·Xaa_6]	[AcNH-Xaa_6-Dbo]	[AcNH-FTrp-Xaa_6]
Peptides (Only Asp_6) with Acetylated N-Terminus (Only C-Terminal Charges Possible)		
AcNH-FTrp-Asp_6-Dbo-COOH	AcNH-Asp_6-Dbo-COOH	AcNH-FTrp-Asp_6-COOH
[Ac·Asp_6·COOH]	[- - -]	[- - -]

[a]Short notation used in the main text and in Figure 4. [b]Dbo-only reference peptide required for CIFQ. [c]FTrp-only reference peptide required for sdFRET.

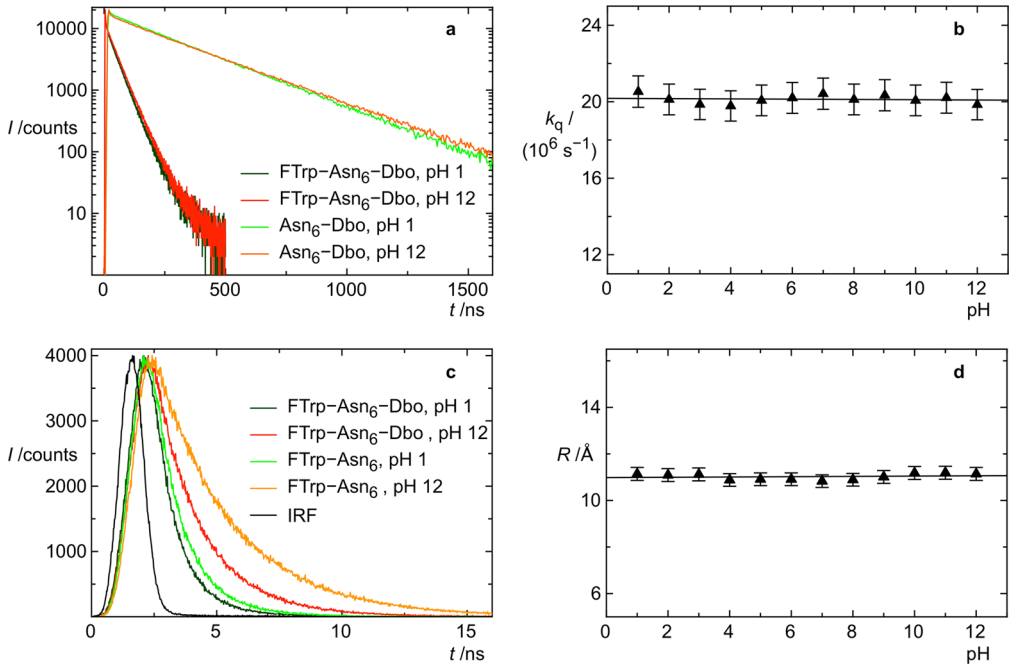

Figure 3. (a) CIFQ: Fluorescence decay profiles of Dbo in FTrp-Asn_6-Dbo at pH 1 (dark green) and pH 12 (red) and in the reference peptide Asn_6-Dbo at pH 1 (green) and pH 12 (orange). (b) The collision rate of FTrp-Asn_6-Dbo plotted against the solution pH. (c) Fluorescence decay profiles of FTrp in FTrp-Asn_6-Dbo at pH 1 (dark green) and pH 12 (red) and in the reference peptide FTrp-Asn_6 at pH 1 (green) and pH 12 (yellow). The instrument response function (IRF, black trace) was routinely recorded for data deconvolution. (d) The resulting effective donor–acceptor distance in FTrp-Asn_6-Dbo plotted against the solution pH; see text for analysis.

$k_q = 1/\tau_D - 1/\tau_S$.[18] The collision rate remained constant at ca. 20×10^6 s^{-1}, the time constant ($1/k_q$) at ca. 50 ns (Figure 3b).

In sdFRET measurements, the kinetic traces at pH 1 and 12 could not coincide (Figure 3c) because the quantum yield and fluorescence lifetime of the donor, FTrp, depend on pH (Supporting Information Figure S2). We obtained the rate constant of FRET, $k_{FRET} = 1/\tau_D - 1/\tau_S$, by using now the FTrp-only labeled peptide as reference. On the basis of Förster's theory, this rate can be directly translated into an effective donor–acceptor distance, R, by using his central equation, $k_{FRET} = (1/\tau_S) \times (R_0/R)^6$. Here, both the natural donor lifetime τ_S, in the absence of acceptor, and the Förster radius, R_0, depend on the donor quantum yield, while the FRET rate constant does not as the combined dependencies cancel out.[10] Thus, the factor R_0^6/τ_S does not change with the quantum yield, and the value of R_0 can be obtained at any pH from the reported values at pH 7.0 ($R_{0,ref} = 9.6$ Å, $\tau_{S,ref} = 2.0$ ns) and from the measured lifetime, τ_S, via $R_0 = R_{0,ref} \times (\tau_S/\tau_{S,ref})^{1/6}$.[10]

Despite the pH-dependency of the fluorescence kinetics, the extracted effective distances between FTrp and Dbo in Asn_6 displayed a remarkable constancy with a value of ca. 11 Å over the entire range of pH values (Figure 3d), consistent with the pH-independent collision dynamics obtained by CIFQ (Figure 3c). This observed absence of pH effects for nonionizable side chains demonstrates that any pH-induced response of ionizable chains has to be traced back to an altered side chain charge status.

Disparity in the Response to Ionization of Acidic and Basic Chains. The pH range from 1 to 12 ensures the complete transition from uncharged to charged side chains in all peptides with the exception of Arg_6 and Lys_6 (pK_a: Asp 3.9, Glu 4.3, Arg 12.5, Lys 10.8, His 6.0).[24,25] The results from all chains are shown in Figure 4 with CIFQ measurements on the left and sdFRET measurements on the right, going from the acidic peptides, Asp_6 and Glu_6, to the basic chains, Arg_6, Lys_6, and His_6. The acidic and basic chains displayed profoundly different patterns. The collision rate and effective distance of

dx.doi.org/10.1021/jp508263a | J. Phys. Chem. B 2015, 119, 33–43

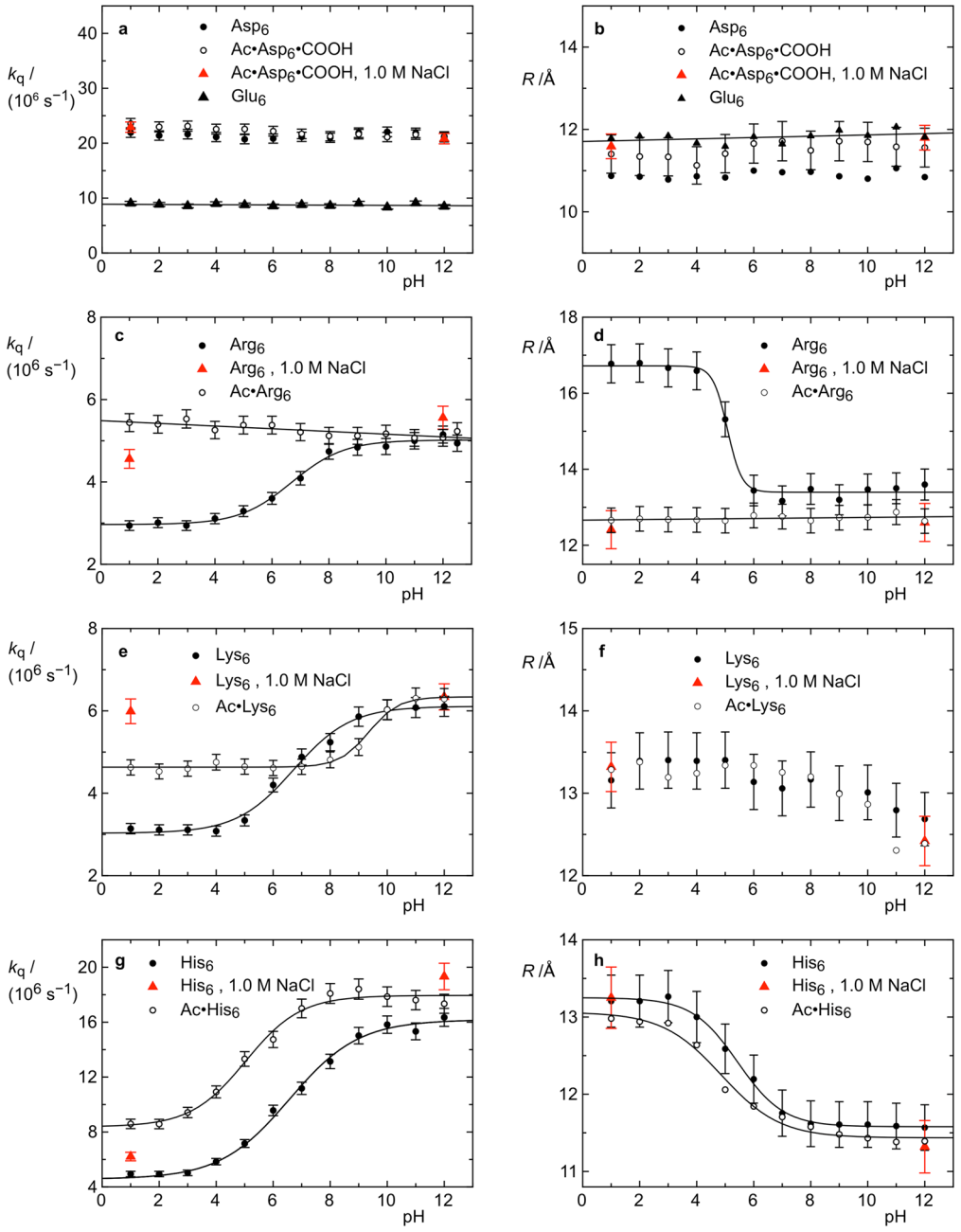

Figure 4. Collision rate, k_q, obtained from CIFQ measurements (left) and the effective distance, R, obtained from sdFRET measurements (right), plotted against the solution pH (a–h) for Xaa_6 chains, for Ac·Xaa_6 chains, for the Ac·Asp_6·COOH peptide (a,b), and in the presence of salt (1.0 M NaCl, red). See also Supporting Information Figures S4–6.

the acidic peptides remained constant over the entire pH range, while the basic chains showed a rich variety of CIFQ and sdFRET profile combinations.

The absence of any charge effect in the acidic chains came as another surprise, and we had to assume an involvement of the N-terminus. Coulomb repulsion between negatively charged side chains could have been offset by favorable interactions between the side chains and a positively charged N-terminus. We disproved this possibility by using a peptide with blocked N- and unblocked C-terminus, AcNH-FTrp-Asp_6-Dbo-COOH (Ac·Asp_6·COOH, Table 1), again expecting that it could make a difference when seven negative charges appear on seven adjacent residues. Yet, again, the pH profiles remained horizontal (Figure 4a,b; Table 2).

Salt Effects. A common test for Coulomb repulsion between like-charged groups is whether the putative effects disappear in the presence of salt. A clear indication that repulsion controls chain dimensions is chain compaction in salt presence.[2,8] Like-charged side chains can be nearest neighbors along the chain but can still come closer when any strain caused by repulsion is neutralized by salt. Following Debye–Hückel theory, salt addition can shorten the Debye length, that is, the distance above which repulsion becomes ineffective, to less than 2 Å,[26] a distance that is short even for neighboring charged residues. Interestingly, salt effects (with 1.0 M NaCl, at low pH for the basic chains and high pH for the acidic chains) afforded quite different responses; that is, the collision rate showed a factor of 2 increase for Lys_6, 50% increase for Arg_6, 25%

dx.doi.org/10.1021/jp508263a | J. Phys. Chem. B 2015, 119, 33–43

Table 2. Collision Rate Constants and Effective Donor–Acceptor Distances at Low and High pH

	$k_q/(10^6\ s^{-1})^{a,b}$		$R/Å^{a,c}$		$R_{MD}/Å$ (charge status)^d	
peptide chain	pH < 2	pH > 11	pH < 2	pH > 11	protonated	unprotonated
Asn_6	20	20	10.9	11.0	13.0 (+1)	12.4 (+0)
Asp_6	22	22	10.9	11.0	10.0 (+1)	12.5 (−6)
$Ac{\cdot}Asp_6{\cdot}COOH^e$	23	21	11.5	11.6	13.4 (0)	14.4 (−7)
Glu_6	8.9	8.8	11.8	12.0	9.3 (+1)	12.1 (−6)
Arg_6	3.0	5.1	16.8^f	13.5	16.0 (+7)	15.6 (+6)
Arg_6/1.0 M NaCl	4.6	5.6	12.4	12.6		
$Ac{\cdot}Arg_6$	5.4	5.1	12.7	12.8	16.3 (+6)	
Lys_6	3.1	6.1	13.2	12.7	17.5 (+7)	15.5 (+0)
Lys_6/1.0 M NaCl	6.0	6.3	13.3	12.4		
$Ac{\cdot}Lys_6$	4.6	6.3	13.3	12.3		
His_6	4.9	16	13.2	11.6	17.9 (+7)	12.4 (+1)
His_6/1.0 M NaCl	6.2	19	13.3	11.3		
$Ac{\cdot}His_6$	8.6	19	12.9	11.4		

[a]Average of values measured below pH 2 and above pH 11, respectively. [b]±5% error. [c]The error increases exponentially from ±0.15 Å at R = 9.6 Å (R_0) to ±0.8 Å at R = 12.0 Å and ±2.5 Å at R = 17.0 Å. [d]Average end-to-end distance in simulated peptides; charge status given in brackets. [e]The experimental values in the absence and presence of salt (1.0 M NaCl) are virtually identical. [f]Distances outside the range between $0.5R_0$ and $1.5R_0$, where R_0 is 9.6 Å, cannot be determined with high accuracy; the given value constitutes a lower limit.

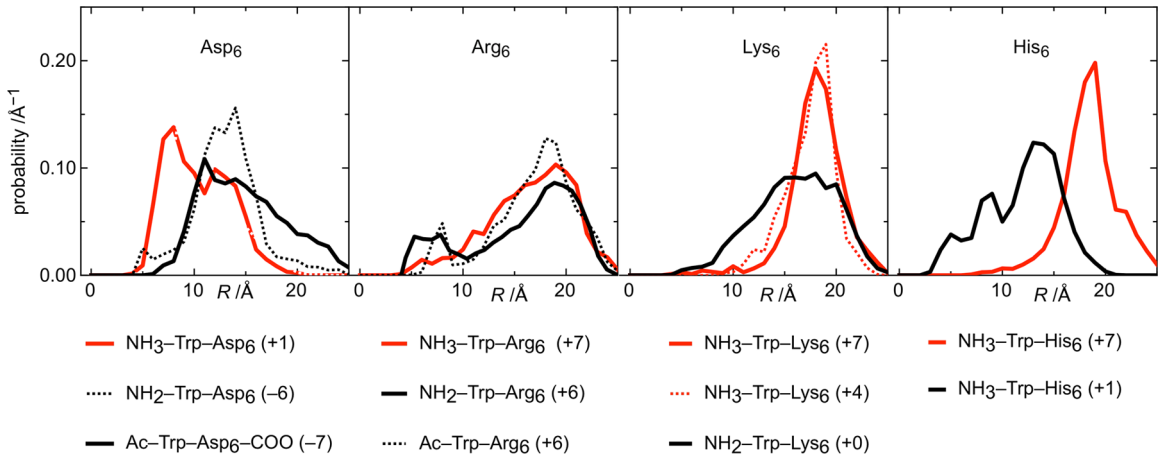

Figure 5. Distance distributions of the acidic and basic peptides with varying charge status. The distributions were obtained from end-to-end distance trajectories of at least 200 ns duration. The end-to-end distance was measured from the N-terminus (center of the central C–C bond of the indol ring) to the carbon atom of the C-terminal carboxyl group.

increase for His_6, but no effect for Asp_6 and Glu_6 (Table 2, Figure 4, Supporting Information Figures S3–5). The effective distance, in contrast, was affected only for Arg_6 (Figure 4d).

MD Simulations. Confronted with the apparent absence of any charge repulsion between negatively charged side chains in homorepeat peptides in water, we questioned common chemical intuition and tested whether the physical models used in MD simulations (MD) could effortlessly predict the absence of any Coulomb effects in acidic chains. Thus, we simulated representative peptide sequences that we studied experimentally by using Amber 11 and the Amber ff99SB force field,[27,28] routine but state-of-the-art MD tools that were, for instance, successfully employed in protein-folding thermodynamic predictions.[29]

Because absolute quantitative agreement could not be expected (see below), but at best an agreement between experimental and theoretical trends with pH and side chain charge status, we accepted two simplifications to bypass parametrization inconsistencies; the simulated chains contained Trp instead of FTrp, and they contained no C-terminal Dbo. Akin to our previous studies,[12,15] water was modeled explicitly, and the simulations were run for at least 200 ns to ensure convergence. The average end-to-end distances, R_{MD}, obtained from the distance distributions (Figure 5), and in particular their pH dependence, can be compared to the effective distances extracted from the sdFRET experiments (Table 2). Note that these experimental distances are systematically slightly smaller than the real average distance because of the higher contribution of short distances to FRET.[10,11] Thus, also the MD-calculated average distances tend to be larger than the experimental values.

The MD simulations predicted an impact of side chain charges for all peptides (Figure 5). When we performed a comprehensive cluster analysis of all systems based on ref 30 (Supporting Information Appendix) and also analyzed the probabilities of transient intrachain hydrogen bonds (Supporting Information Table S1), we were led to critical short-distance conformations (Figure 6a–f).

DISCUSSION

While it is broadly accepted that electrostatic repulsion can impact the thermodynamic stability of globular proteins,[31,32] its

dx.doi.org/10.1021/jp508263a | J. Phys. Chem. B 2015, 119, 33–43

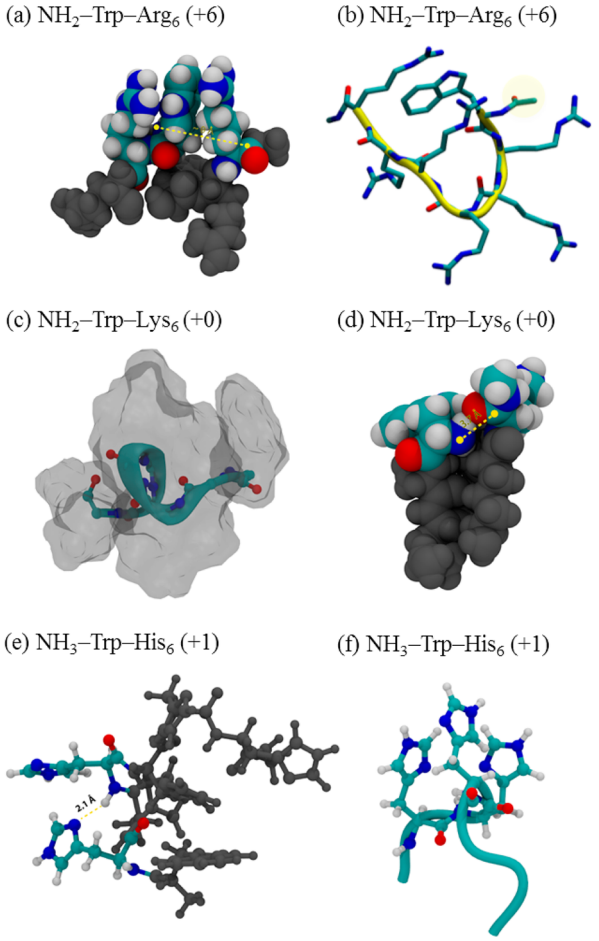

Figure 6. Short-distance structures of basic peptides. (a,b) The π-cation interactions in Arg_6 induce short distances (9 Å) by stabilizing an arginine-tryptophan-arginine sandwich conformation. (c) Hydrophobic, neutral lysine side chains constitute a low-permittivity environment that stabilizes main chain hydrogen bonds in Lys_6 and (D) favors conformations of short end-to-end distance (6–10 Å). (e) Side chain–main chain and (f) side chain–side chain hydrogen bonds in His_6.

dominant role in determining the spatial dimensions of flexible IDPs including arginine-rich antimicrobial peptides, protamine peptides, and human prothymosin α has been investigated only recently.[1,2] We have now tackled the fundamental understanding of charge effects in proteins in a bottom-up-approach, by investigating short polypeptides exclusively composed of the same ionizable side chains, Asp, Glu, Lys, Arg, Lys, and His. The experimental parameters that we recorded were the effective end-to-end distance and collision rate, as a measure of chain structure and flexibility. Foregoing to any interpretation of pH-caused charge effects, it is important to discuss how distances and collision rates vary between the different types of amino acid residues.

Dependence of End-to-End Distances and Collision Rates on the Amino Acid Type. Obvious factors that dominate differences in end-to-end distances of homorepeat peptides are side chain–side chain excluded-volume effects and the maximization of side chain entropy that is achieved when the main chain expands.[17,33−36] Accordingly, the average length of a peptide increases when the steric bulk and the length of a side chain increase. The same reasons dictate the end-to-end collision rates. The side chains of Arg, Lys, and His occupy a larger volume than the acidic side chains, Asp and Glu, and those of Arg and Lys are also "longer" in the sense that they possess 3−4 instead of 1−2 flexible methylene groups. Indeed, the effective end-to-end distances extracted from the experiments (Table 2, Figure 4) for the "bigger" side chains, Arg (ca. 17 Å at pH 2) and His and Lys (ca. 13 Å at pH 2), are significantly longer than those for the "smaller" ones, Asn and Asp (ca. 11 Å) and Glu (ca. 12 Å). Note that even the small difference between Glu and Asp/Asn (one additional methylene group for Glu) is nicely reflected in a ca. 1 Å larger distance. The MD calculations afforded consistent results, that is, shorter average distances for the acidic amino acids (Table 2). The trends of the end-to-end collision rates (Table 2, Figure 4) can also be roughly rationalized in part through steric effects;[17] for example, basic chains display smaller rates than acidic chains, and the collision rate for Glu is a factor of 2 less than that for Asp/Asn.

While the consistency of the trends of the end-to-end distances and collision rates with the type of amino acid is reassuring for the employed experimental and theoretical approaches, they have also important implications for the charge effects that could be expected. If side chain bulk and entropy cause larger end-to-end distances and slower end-to-end collision rates of the chain, electrostatic repulsion between the side chains should also become less effective. Therefore, the most prominent effects of charge repulsion were expected for the shortest peptides, those composed of the acidic Asp_6 and Glu_6 backbone, but, strikingly, exactly these side chains turned out to be immune, as far as their dynamics and end-to-end distances were concerned, toward charge and pH effects (Table 2, Figure 4).

pH Independence for Acidic Hexapeptides. The Asp and Glu hexamers displayed almost constant end-to-end collision rates (within ±5%) and effective end-to-end distances (within ±0.5 Å) at every pH between 1 and 12 (Figure 4a,b). This result, obtained by two photophysically independent kinetic methods, CIFQ and sdFRET, and pointing to the absence of charge repulsion in highly negatively charged short peptide chains, could not have been anticipated: In MD simulations, deprotonation stretched Asp_6/Glu_6 from 10.0 Å/9.3 Å to 12.5 Å/12.1 Å by 2.5 Å/2.8 Å (Table 2), which is a significant fraction of the maximal 10-Å stretching that we obtained, when we placed artificially high charges on the Asp_6 carboxylate groups, to obtain a reference value. On the other hand, when the N-terminus was neutralized, acetylated, as in Ac·Asp_6·COOH, the pH-induced deprotonation led to a stretching of merely 1.0 Å, from 13.4 to 14.4 Å. This larger value of 13.4 Å in contrast to the value of 10.0 Å in protonated Asp_6 suggests that it is not so much Coulomb repulsion that was poorly represented in the MD simulations but, instead, the strength of interactions between the charged N-terminal ammonium group of Asp_6 and its chain. Indeed, it is exactly this idea, which is reinforced, when we later turn to the basic chains.

In pertinent studies, Buscaglia and co-workers replaced three glutamine residues of a 14-mer peptide for glutamate, Cys-(Ala-Gly-Gln)$_4$-Trp → Cys-(Ala-Gly-Glu)$_4$-Trp, and measured the Förster energy transfer between Trp and Dansyl-labeled Cys.[37] Also here, the additional charges, but on residues well separated along the chain, did not affect the end-to-end intrachain distance. Schweitzer-Stenner and co-workers studied the extremely short trimer Asp_3 at varying pH. The required methods, vibrational CD, UV-CD, and ^{1}H NMR spectroscopy,

dx.doi.org/10.1021/jp508263a | J. Phys. Chem. B 2015, 119, 33−43

allowed a multitude of conclusions, among them a conformational response of the central aspartate side chain, but no simple extrapolation to intrachain collision rates and distances.[38]

We also considered whether the horizontal pH profiles of the acidic chains could be caused by different influences that exactly compensate each other. When the chain becomes charged, it might expand, but intrachain diffusion might increase. While chain expansion would lead to a reduced collision frequency and increased effective distance, enhanced diffusion would effect the reverse. It is admittedly improbable that the net result would be zero over the entire pH range, but, to address this remote possibility, we included a study of salt effects (1.0 M NaCl, Table 2, Supporting Information Figures S4−6), because the end-to-end collision rates as well as effective distances should be systematically affected if Coulomb repulsion was dominant. Salt addition raises the solution viscosity by merely 2% (1.0 M NaCl) such that viscosity effects on intrachain diffusion, that is, on the collision rate and the effective distance, can be ignored. It is all the more intriguing that the acidic peptides displayed exactly the same rates and distances in the absence and presence of salt. With the combined results of pH and salt independence, we could now conclude with confidence that Coulomb repulsion in short acidic chains affects neither their end-to-end dimensions nor their end-to-end dynamics.

The observed insensitivity toward pH is consistent with the classical concept suggested by Flory, that long linear polymers can be viewed as a sequence of short segments, as "blobs", whose conformational equilibria do not respond to exterior conditions, neither to the chemical nature of the solvent nor to changes of the solution pH.[39,40] While this approximation, the inertia of a blob, is valuable in the treatment of long chains,[41,42] it is insufficient when we try to understand the many facets of peptide chain segments, as our work demonstrates. It would be equally justified to adopt the opposite point of view and argue with Manning's theory of counterion condensation.[43−47] Here, a polyelectrolyte, for instance, the DNA duplex, is modeled as a rigid rod. If the Manning parameter, $q_0 = l_B/l$, that is, the ratio of the Bjerrum length (l_B, ∼7.0 Å at room temperature) and the distance between adjacent charges, l, is greater than unity ($q_0 > 1$), the system is only predicted to be stable in the presence of counterions that, at low salt concentration, would condense onto the chain.[46] The condensation of bivalent counterions is predicted already for $q_0 > 0.5$. However, our experimental procedures warranted a total concentration of mono- and bivalent counterions, even at extreme pH (pH 1.0), of maximally 0.6 μM (cationic) and 6.5 μM (anionic) as compared to 50 μM of peptide. In our simulations, the average distance between adjacent aspartate carboxylates in neutral and charged chains was 7 and 8 Å, respectively, such that condensation of monovalent ions is, according to the theory, not enforced ($q_0 \approx 1$). Measurements in the presence of 1.0 mM EDTA at low and high pH afforded the same results as in its absence (results not shown). When we intentionally added 100 mM calcium chloride to an Asp_6 solution at pH 12.0, we did not observe a chain collapse. Instead, we observed an increased effective distance, possibly as the consequence of repulsion between carboxylate-bound calcium ions (data not shown). This is in line with the investigations of Haber-Pohlmeier et al. on the Ca^{2+} affinity of glutamate-rich sequences, including polyglutamic acid. These authors also detected no counterion condensation at very low Ca^{2+} concentrations and only low-affinity binding at higher ones.[48]

Electrostatic Effects Increase with Increasing Chain Length. How can Coulomb repulsion determine the spatial dimension of an IDP of 20−100 residues, for instance, of the acidic chain of human prothymosin α,[2] when it has no effect on short acidic peptides? Prothymosin α (110 aa) contains not only Asp and Glu but also polar and hydrophobic residues (∼50%). The result is a reduced dielectric permittivity of the charge-surrounding space, which could be a precondition for sufficiently strong and chain-stretching Coulomb forces. However, Duhamel and co-workers studied electrostatic repulsion versus hydrophobicity, varied the fractions of Asp and Phe in long Asp/Phe polymers, and could clearly identify effective Coulomb repulsion in the pure Asp polymer chain.[49]

With increasing length, the chain itself begins, by mere stochastics, to constitute a microenvironment of its own charged side chains. The number of charge-surrounding and solvating water molecules is reduced and, by that, the dielectric permittivity. The repulsive Coulomb energy between the charges increases, as does the desolvation "penalty", to accommodate a charge at low permittivity.[50−52] As a consequence, the chain is forced to expand. To strengthen this hypothesis, we evaluated equilibrium structures obtained from simulations of neutral chains containing 6 or 30 protonated aspartate residues. An approximate model[42] afforded average apparent dielectric constants of 33 for Asp_6 and 10 for Asp_{30}, that is, a 3 times higher Coulomb energy and desolvation penalty for Asp_{30} (see the Supporting Information for details). This large difference guarantees that, after deprotonation and complete side chain ionization, Asp_{30} expands dramatically, in contrast to Asp_6.

In recent simulations, Ramachandran et al. compared the neutral and charged states of the Asp_{10} decamer and Asp_{30} tricosamer.[53] The end-to-end distance in Asp_{10} almost doubled upon deprotonation, while it increased about 5-fold in Asp_{30} (see p 13909 in Table 1 of ref 53). These results underline our point, although it is slightly surprising that the decamer expands significantly while the hexamer that we studied shows no response in the experiments and only a modest one in the simulations. Our production runs extended over 200 ns, while the runs of Ramachandran et al. extended over only 50 ns, which might not be sufficient, particularly, when we consider that the experimental time constant of end-to-end collision ($1/k_q$) is already 45 ns (Table 2) in the shorter Asp_6 chain and that it will be even larger in the Asp_{10} chain.[18]

In conclusion, dielectric-permittivity arguments are likely a dominant cause of the strong response to charge repulsive effects in longer acidic peptides or IDPs, but they cannot explain why the MD simulations predict modest but sizable differences for short chains, while experimentally no effect is found. We therefore evaluated the robustness of the MD simulations and varied the explicit water solvent model, going from the TIP3P[54] to the succeeding TIP4P model.[55] However, the chain expanded even more (from 14.4 to 18.5 Å, Figure 7). Although this trend can be rationalized by the discrepant dielectric constants of water predicted by the models, 82 for TIP3P and 50 for TIP4P,[56] it impressively illustrates that systematic shortcomings of MD methods can still not be ruled out.

Searching for factors that are potentially critical but ignored in MD simulations, we focused on specific-ion effects. It has, for instance, been established that the carboxylate group binds water molecules tightly, with an apparent hydration number of two.[57−61] When we suppressed the exchange of carboxylate-

dx.doi.org/10.1021/jp508263a | J. Phys. Chem. B 2015, 119, 33−43

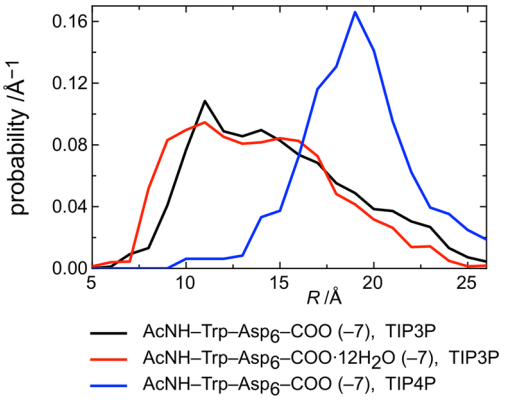

Figure 7. MD-simulated end-to-end distance distributions of hexaaspartate in its deprotonated state (−7) in the absence (black) and presence (red) of constraints: In the simulation of the peptide AcNH-Trp-Asp_6-COO·$12H_2O$ (−7), the exchange of side chain-bound water molecules with bulk water was suppressed. Also shown is the effect of the explicit water solvent models TIP3P (black, red) and TIP4P (blue) on the distance distributions.

bound water molecules with bulk water in the simulations (Supporting Information Figure S8), the distance distribution shifted toward shorter distances (Figure 7), and the resulting average distance of 13.4 Å did indeed coincide with that of the neutral Ac·Asp_6·COOH chain. This distance is still significantly larger than that of the Asp_6 chain with neutral side chains but charged N-terminus (10.0 Å, Table 2). There are likely to be additional factors, which are slightly misrepresented in the force-field calculations. In the neutral Asp_6 chain, the strength of intrachain interactions between the ammonium group and the chain is probably overestimated, while, in the charged chain, the charge distribution within the carboxylate−water clusters is ignored, because the negative charge is a priori localized on the carboxylate oxygen atoms. As it stands, the proper treatment of carboxylate hydration is still under debate.[62,63]

pH Dependence for Basic Hexapeptides. In sharp contrast to the acidic hexapeptides, the basic ones (Arg, Lys, His) all displayed a significant pH dependence of the end-to-end collision rates and distances in the experiments as well as the MD simulations (Table 2, Figure 4c−h). In detail, their end-to-end collision rates in their low-pH, positively charged forms, were lower and their effective end-to-end distances were larger. While it is tempting to attribute this trend to Coulomb forces, its absence in the acidic peptides called for extensive control experiments.

The end-to-end flexibility of hexaarginine and -lysine almost doubled when the pH was raised (Figure 4c,e). The very similar transitions started at about pH 6 and had to be due to the deprotonation of the free N-terminal ammonium group ($pK_a \approx 7.7$); the side chains titrate much later (Arg $pK_a \approx 12.5$, Lys $pK_a \approx 10.5$).[64] Indeed, when we acetylated the N-terminus of Arg_6, the collision rate remained constantly at high values over the entire pH range. When we acetylated the N-terminus of Lys_6, a low-amplitude transition at higher pH was still detectable and could only be caused by deprotonation of lysine side chains. Moreover, adding salt increased the collision rate of free-N-terminus Arg_6 and Lys_6 as effectively as raising the pH and had no effect at high pH, where N-terminal neutrality is guaranteed (pH > 9.0, Figure 4c−e; Supporting Information Figures S5, 6).

As has been mentioned and is known from other contact-quenching methods,[37] the end-to-end flexibility of chains is highly sensitive to attractive/repulsive interaction forces that act on probes in proximity. Hence, there is no surprise in that a charged N-terminal FTrp can energetically favor or disfavor chain structures with contacting ends. Such looped conformations are necessarily more compact than relaxed and better solvated conformations and display an accordingly smaller dielectric permittivity. The increased effectiveness of Coulomb repulsion between the N-terminal ammonium group and the arginine and lysine side chains or, simply, the penalty to be paid for a charged group to stay in a low-permittivity environment could explain the low end-to-end flexibility observed at low pH.

Förster energy transfer, on the other hand, takes place at all distances; even when the probabilities of distances, at which probes are almost in direct contact, vary strongly, if they remain small in comparison to the probabilities of nonstrained conformations, they can hardly be detected by sdFRET. Indeed, the FRET profile of Lys_6 (as well as N-acetylated Lys_6) indicated only a marginal structural change, which became more visible at high pH values (Figure 4f), at which the lysine side chains are expected to become neutral. MD prediction almost coincided with these experimental observations. Upon going from the protonated to the neutral hexalysine chain, the distance distribution broadened due to an increase of short-distance probability (Figure 5), as was experimentally reflected by a collision-rate increase. The peak and average distances, however, changed only mildly (from 17.5 to 15.5 Å, Table 2), which was reasonably reflected by the small (0.7 Å) decrease in the sdFRET measurements reporting on the entire distribution of distances. Side chain neutralization favored hydrophobic as well as intramain chain interactions due to the considerable hydrophobicity of the lysine butano spacers and the accompanying decrease of dielectric permittivity, at which transient helical segments and short-distance conformations became slightly more stable (Figure 6c,d).

In view of the foregoing discussion, the second surprise of our study was the large and sharp structural transition of the Arg_6 peptide (Figure 4d). Its chain displayed the largest effective end-to-end distance among the peptides (16.8 Å at low pH, Table 2), which strictly depended on the presence of a charged N-terminus. When the N-terminus was neutralized (by acetylation or at high pH) or when salt was added, the chain collapsed by about 3 Å (Figure 4d). Hence, again, the experiments yielded only little indication for side chain−side chain Coulomb repulsion (13.5 Å in the absence and 12.6 Å in the presence of 1.0 M NaCl, Table 2) but rather for a repulsion between the N-terminal ammonium group and the charged side chain units or, simply, for the penalty to be paid for a charged group located in a low-permittivity environment.

The MD simulations of Arg_6 with charged guanidinium units and neutral N-terminus were the only ones that did not converge within 500 ns. The distance trajectory pointed to a remarkably stable short-distance subpopulation (Supporting Information Figure S9). In a representative compact structure with an end-to-end distance of only 9 Å, two arginine residues were stacked to the two sides of the tryptophan indol ring (Figure 6c,d). Note that the indole−guanidinium interaction is the strongest among the familiar cation-π interactions between basic and aromatic side chains.[65] The stability of the cation-π stacked complexes decreases when the N-terminal FTrp becomes itself positively charged, for reasons of competitive binding of the terminal $-NH_3^+$ group as well as charge repulsion of adjacent charges, resulting in a more expanded chain distribution, as observed experimentally and theoretically.

dx.doi.org/10.1021/jp508263a | J. Phys. Chem. B 2015, 119, 33−43

The Arg_6 experiments expose once again the N-terminus as a potentially important denominator of the structural and dynamic properties of peptides and of their biological activity; another prominent example is α-synuclein, abundant in the human brain and involved in Parkinson's disease.[66−68]

pH Dependence for Hexahistidine. Among the basic residues, histidine is closest to glutamate and aspartate with side chains of six, five, and four heavy atoms. Yet, in contrast to the acidic peptides, the collision rate of His_6 increased and the effective distance decreased between pH 4 and 8, which could easily be ascribed to a reduced Coulomb repulsion and concomitant chain contraction. The corresponding MD simulations were qualitatively in agreement but exaggerated the compaction: The average distance decreased from 17.9 to 12.4 Å, by more than 5 Å (Table 2; a reasonable explanation is suggested in the Supporting Information, section 10).

While pH-dependent Coulomb forces seemed to dominate the CIFQ and sdFRET pH profiles of His_6, the observed effective distances remained unchanged when salt was added. These apparently contradictive observations can be reconciled: Instead of focusing on neutral and spatially separated side chains that, when they become charged, separate even more and stretch the chain, we can consider neutral side chains that interact and bind to each other and to the backbone and keep the chain in compact conformations. Such contacts disappear when the contact partners become charged by protonation, but in a salt-independent manner. Recent studies are in support of this concept and suggest that the imidazole rings of two neutral histidine side chains can form transient hydrogen bonds and also $\pi-\pi$ stabilized contact pairs with one ring stacked upon the other.[69−72] In addition, the MD simulations indicated significantly increased main chain−side chain interactions in neutral His_6 (Supporting Information Table S1); only the neutral imidazole ring can act as both hydrogen-bond donor and acceptor for the peptide backbone. In summary, the His_6 peptide experiences an apparent compaction upon deprotonation due to increased specific intrachain interactions, which accounts for the fact that the effective end-to-end distance is rather insensitive to the presence of salts, but nevertheless sensitive to pH.

CONCLUSIONS

Coulomb repulsion plays no or a remarkably small role in highly charged but well solvated peptide chains such as hexaaspartate and -glutamate. It is, however, effective at contact distance when it disrupts side chain−side chain and side chain−main chain interactions in hexahistidine and when it disfavors the looped and compact conformations of hexaarginine and -lysine probed by CIFQ. The charged N-terminus is kept apart from the low-permittivity volume of the chain body. This result is counterintuitive for the human but less counterintuitive for the machine; MD simulations predict sizable but modest effects. We demonstrated the synergy and efficiency of the fluorescence methods sdFRET and CIFQ that can test the structure and flexibility of the short peptide, but can potentially diagnose any developing short-distance relationship, for instance, during protein folding or enzymatic activity.

MATERIALS AND METHODS

Materials. All peptides were synthesized in cooperation with Biosyntan (Berlin) and were obtained in >95% purity. We prepared the Fmoc derivative of Dbo and of 5-fluoro-L-tryptophan as previously described.[18] In their standard form, the peptides had a free N-terminus (NH_2-/NH_3^+-) and amidated C-terminus ($-CONH_2$); variations from this pattern are indicated in the main text. All chemicals were purchased from Sigma-Aldrich.

Spectroscopy. The fluorescence lifetimes of all peptides were measured by time-correlated single-photon counting (FLS920, Edinburgh Instruments Ltd.) at a fixed temperature of 25 °C (Julabo F25/HD thermostat) and peptide concentrations of ca. 50 μM. The solution pH was adjusted by adding HCl or NaOH; the pH values remained as initially set, as was routinely confirmed by pH determination after measurement.

In sdFRET measurements, the tryptophan residue was excited at 280 nm by using a pulsed LED (PicoQuant, PLS-280, fwhm ca. 300 ps), and tryptophan fluorescence was followed at 350 nm. The Förster radius of the FTrp/Dbo pair was determined as previously described.[10] The instrument response function was routinely recorded and used in deconvolution. In CIFQ measurements, Dbo was excited at 373 nm by using a diode laser (PicoQuant, LDH-P-C 375, fwhm ca. 50 ps), and Dbo fluorescence was followed at 450 nm.

Molecular Dynamics Simulations. The simulated peptides contained a C-terminal Trp residue (instead of FTrp) and contained no N-terminal Dbo (to bypass parametrization inconsistencies). In their standard form, peptides had a free N-terminus (NH_2-/NH_3^+-) and a methylamidated C-terminus ($-CONHCH_3$); variations from this pattern are indicated in the main text. We used the AMBER 11 program with the Amber ff99SB force field.[27,28] The trajectories were visualized by using the VMD software package[73] and were analyzed by using the PTRAJ module of AMBER, followed by a cluster analysis based on the average-linkage algorithm with a 3.0 Å cutoff value on a total of 2500 conformations sampled from the simulation, one per every 80 ps.[30] See the Supporting Information for further details.

ASSOCIATED CONTENT

Supporting Information

(1) Collisional quenching of DBO by FTrp (Figure S1). (2) pH-dependent fluorescence lifetime of 5-fluoro-L-tryptophan (Figure S2) and time-resolved fluorescence decays of FTrp-Lys_6-Dbo and FTrp-Lys_6 (Figure S3). (3) CIFQ measurements in the presence of salt (Figures S4−6). (4) Temperature dependence of CIFQ in hexahistidine (Figure S7). (5) Apparent dielectric constants in Asp_6 and Asp_{30}. (6) Details of MD simulations. (7) Transient hydrogen bonds in MD simulations (Table S1). (8) Simulation of an acidic chain with tightly bound water (Figure S8). (9) Indications from MD simulations of two-state folding behavior in hexaarginine (Figure S9). (10) The hexahistidine collapse exaggerated in MD simulations. Appendix: Representative structures from cluster analysis. This material is available free of charge via the Internet at http://pubs.acs.org.

AUTHOR INFORMATION

Corresponding Authors

*Phone: +49-421-2003233. E-mail: m.jacob@jacobs-university.de.

*E-mail: w.nau@jacobs-university.de.

Notes

The authors declare no competing financial interest.

■ ACKNOWLEDGMENTS

We thank Indrajit Ghosh for preliminary measurements, and Achim Geleßus, Danilo Roccatano, and Ulrich Kleinekathöfer for MD discussions. The Deutsche Forschungsgemeinschaft (DFG, NA 686/6) supported this work. A.N., S.Z., and K.I.A. thank the DAAD for financial support.

■ REFERENCES

(1) Mao, A. H.; Crick, S. L.; Vitalis, A.; Chicoine, C. L.; Pappu, R. V. Net Charge Per Residue Modulates Conformational Ensembles of Intrinsically Disordered Proteins. *Proc. Natl. Acad. Sci. U.S.A.* **2010**, *107*, 8183−8188.

(2) Müller-Späth, S.; Soranno, A.; Hirschfeld, V.; Hofmann, H.; Ruegger, S.; Reymond, L.; Nettels, D.; Schuler, B. Charge Interactions Can Dominate the Dimensions of Intrinsically Disordered Proteins. *Proc. Natl. Acad. Sci. U.S.A.* **2010**, *107*, 14609−14614.

(3) Marsh, J. A.; Forman-Kay, J. D. Sequence Determinants of Compaction in Intrinsically Disordered Proteins. *Biophys. J.* **2010**, *98*, 2383−2390.

(4) Uversky, V. N.; Oldfield, C. J.; Dunker, A. K. Intrinsically Disordered Proteins in Human Diseases: Introducing the D2 Concept. *Annu. Rev. Biophys.* **2008**, *37*, 215−246.

(5) Uversky, V. N.; Dunker, A. K. Understanding Protein Non-Folding. *Biochim. Biophys. Acta* **2010**, *1804*, 1231−1264.

(6) Ganguly, D.; Zhang, W. H.; Chen, J. H. Electrostatically Accelerated Encounter and Folding for Facile Recognition of Intrinsically Disordered Proteins. *PLoS Comput. Biol.* **2013**, *9*, e1003363.

(7) Hofmann, H.; Nettels, D.; Schuler, B. Single-Molecule Spectroscopy of the Unexpected Collapse of an Unfolded Protein at Low pH. *J. Chem. Phys.* **2013**, *139*.

(8) Hofmann, H.; Golbik, R. P.; Ott, M.; Hübner, C. G.; Ulbrich-Hofmann, R. Coulomb Forces Control the Density of the Collapsed Unfolded State of Barstar. *J. Mol. Biol.* **2008**, *376*, 597−605.

(9) Huang, F.; Lerner, E.; Sato, S.; Amir, D.; Haas, E.; Fersht, A. R. Time-Resolved Fluorescence Resonance Energy Transfer Study Shows a Compact Denatured State of the B Domain of Protein A. *Biochemistry* **2009**, *48*, 3468−3476.

(10) Jacob, M. H.; Dsouza, R. N.; Ghosh, I.; Norouzy, A.; Schwarzlose, T.; Nau, W. M. Diffusion-Enhanced Förster Resonance Energy Transfer and the Effects of External Quenchers and the Donor Quantum Yield. *J. Phys. Chem. B* **2013**, *117*, 185−198.

(11) Jacob, M. H.; Nau, W. M. In *Folding, Misfolding and Nonfolding of Peptides and Small Proteins*; Schweitzer-Stenner, R., Ed.; John Wiley & Sons: NJ, 2012.

(12) Sahoo, H.; Roccatano, D.; Hennig, A.; Nau, W. M. A 10-Angstrom Spectroscopic Ruler Applied to Short Polyprolines. *J. Am. Chem. Soc.* **2007**, *129*, 9762−9772.

(13) Sahoo, H.; Nau, W. M. Phosphorylation-Induced Conformational Changes in Short Peptides Probed by Fluorescence Resonance Energy Transfer in the 10 Angstrom Domain. *ChemBioChem* **2007**, *8*, 567−573.

(14) Sahoo, H.; Roccatano, D.; Zacharias, M.; Nau, W. M. Distance Distributions of Short Polypeptides Recovered by Fluorescence Resonance Energy Transfer in the 10 Angstrom Domain. *J. Am. Chem. Soc.* **2006**, *128*, 8118−8119.

(15) Roccatano, D.; Sahoo, H.; Zacharias, M.; Nau, W. M. Temperature Dependence of Looping Rates in a Short Peptide. *J. Phys. Chem. B* **2007**, *111*, 2639−2646.

(16) Nau, W. M.; Huang, F.; Wang, X. J.; Bakirci, H.; Gramlich, G.; Marquez, C. Exploiting Long-Lived Molecular Fluorescence. *Chimia* **2003**, *57*, 161−167.

(17) Huang, F.; Nau, W. M. A Conformational Flexibility Scale for Amino Acids in Peptides. *Angew. Chem., Int. Ed.* **2003**, *42*, 2269−2272.

(18) Hudgins, R. R.; Huang, F.; Gramlich, G.; Nau, W. M. A Fluorescence-Based Method for Direct Measurement of Submicrosecond Intramolecular Contact Formation in Biopolymers: An Exploratory Study with Polypeptides. *J. Am. Chem. Soc.* **2002**, *124*, 556−564.

(19) Liu, T.; Callis, P. R.; Hesp, B. H.; de Groot, M.; Buma, W. J.; Broos, J. Ionization Potentials of Fluoroindoles and the Origin of Nonexponential Tryptophan Fluorescence Decay in Proteins. *J. Am. Chem. Soc.* **2005**, *127*, 4104−4113.

(20) Sarkar, S. S.; Udgaonkar, J. B.; Krishnamoorthy, G. Reduced Fluorescence Lifetime Heterogeneity of 5-Fluorotryptophan in Comparison to Tryptophan in Proteins: Implication for Resonance Energy Transfer Experiments. *J. Phys. Chem. B* **2011**, *115*, 7479−7486.

(21) Huang, F.; Hudgins, R. R.; Nau, W. M. Primary and Secondary Structure Dependence of Peptide Flexibility Assessed by Fluorescence-Based Measurement of End-to-End Collision Rates. *J. Am. Chem. Soc.* **2004**, *126*, 16665−16675.

(22) Jorda, J.; Kajava, A. V. Protein Homorepeats Sequences, Structures, Evolution, and Functions. *Adv. Protein Chem. Struct. Biol.* **2010**, *79*, 59−88.

(23) Lindorff-Larsen, K.; Piana, S.; Dror, R. O.; Shaw, D. E. How Fast-Folding Proteins Fold. *Science* **2011**, *334*, 517−520.

(24) Arnold, M. R.; Kremer, W.; Lüdemann, H. D.; Kalbitzer, H. R. ^{1}H-NMR Parameters of Common Amino Acid Residues Measured in Aqueous Solutions of the Linear Tetrapeptides Gly-Gly-X-Ala at Pressures between 0.1 and 200 MPa. *Biophys. Chem.* **2002**, *96*, 129−140.

(25) Bundi, A.; Wüthrich, K. ^{1}H-NMR Parameters of the Common Amino-Acid Residues Measured in Aqueous-Solutions of the Linear Tetrapeptides H-Gly-Gly-X-L-Ala-Oh. *Biopolymers* **1979**, *18*, 285−297.

(26) Dill, K. A.; Bromberg, S. *Molecular Driving Forces*; Garland Science: New York, 2011.

(27) Simmerling, C.; Strockbine, B.; Roitberg, A. E. All-Atom Structure Prediction and Folding Simulations of a Stable Protein. *J. Am. Chem. Soc.* **2002**, *124*, 11258−11259.

(28) Hornak, V.; Abel, R.; Okur, A.; Strockbine, B.; Roitberg, A.; Simmerling, C. Comparison of Multiple Amber Force Fields and Development of Improved Protein Backbone Parameters. *Proteins: Struct., Funct., Bioinf.* **2006**, *65*, 712−725.

(29) Day, R.; Paschek, D.; Garcia, A. E. Microsecond Simulations of the Folding/Unfolding Thermodynamics of the Trp-Cage Miniprotein. *Proteins: Struct., Funct., Bioinf.* **2010**, *78*, 1889−1899.

(30) Shao, J. Y.; Tanner, S. W.; Thompson, N.; Cheatham, T. E. Clustering Molecular Dynamics Trajectories: 1. Characterizing the Performance of Different Clustering Algorithms. *J. Chem. Theory Comput.* **2007**, *3*, 2312−2334.

(31) Perl, D.; Müller, U.; Heinemann, U.; Schmid, F. X. Two Exposed Amino Acid Residues Confer Thermostability on a Cold Shock Protein. *Nat. Struct. Biol.* **2000**, *7*, 380−383.

(32) Pace, C. N.; Alston, R. W.; Shaw, K. L. Charge-Charge Interactions Influence the Denatured State Ensemble and Contribute to Protein Stability. *Protein Sci.* **2000**, *9*, 1395−1398.

(33) Chellgren, B. W.; Creamer, T. P. Side-Chain Entropy Effects on Protein Secondary Structure Formation. *Proteins: Struct., Funct., Bioinf.* **2006**, *62*, 411−420.

(34) Trbovic, N.; Cho, J. H.; Abel, R.; Friesner, R. A.; Rance, M.; Palmer, A. G. Protein Side-Chain Dynamics and Residual Conformational Entropy. *J. Am. Chem. Soc.* **2009**, *131*, 615−622.

(35) Creamer, T. P. Side-Chain Conformational Entropy in Protein Unfolded States. *Proteins: Struct., Funct., Genet.* **2000**, *40*, 443−450.

(36) Farhangi, S.; Weiss, H.; Duhamel, J. Effect of Side-Chain Length on the Polymer Chain Dynamics of Poly(Alkyl Methacrylate)S in Solution. *Macromolecules* **2013**, *46*, 9738−9747.

(37) Soranno, A.; Longhi, R.; Bellini, T.; Buscaglia, M. Kinetics of Contact Formation and End-to-End Distance Distributions of Swollen Disordered Peptides. *Biophys. J.* **2009**, *96*, 1515−1528.

(38) Duitch, L.; Toal, S.; Measey, T. J.; Schweitzer-Stenner, R. Triaspartate: A Model System for Conformationally Flexible Ddd Motifs in Proteins. *J. Phys. Chem. B* **2012**, *116*, 5160−5171.

(39) Rubinstein, M.; Colby, R. H. *Polymer Physics*; Oxford University Press: New York, 2003.

(40) Dobrynin, A. V.; M, R. Flory Theory of a Polyampholyte Chain. *J. Phys. II France* **1995**, *5*, 677−695.
(41) Tran, H. T.; Mao, A.; Pappu, R. V. Role of Backbone - Solvent Interactions in Determining Conformational Equilibria of Intrinsically Disordered Proteins. *J. Am. Chem. Soc.* **2008**, *130*, 7380−7392.
(42) Das, R. K.; Pappu, R. V. Conformations of Intrinsically Disordered Proteins Are Influenced by Linear Sequence Distributions of Oppositely Charged Residues. *Proc. Natl. Acad. Sci. U.S.A.* **2013**, *110*, 13392−13397.
(43) Manning, G. S. Limiting Laws and Counterion Condensation in Polyelectrolyte Solutions. 3. An Analysis Based on Mayer Ionic Solution Theory. *J. Chem. Phys.* **1969**, *51*, 3249−3252.
(44) Manning, G. S.; Ray, J. Counterion Condensation Revisited. *J. Biomol. Struct. Dyn.* **1998**, *16*, 461−476.
(45) Stigter, D. Evaluation of the Counterion Condensation Theory of Polyelectrolytes. *Biophys. J.* **1995**, *69*, 380−388.
(46) O'Shaughnessy, B.; Yang, Q. Manning-Oosawa Counterion Condensation. *Phys. Rev. Lett.* **2005**, *94*.
(47) Manning, G. S. Excess Counterion Condensation on Polyelectrolyte Kinks and Branch Points and the Interaction of Skewed Charged Lines. *Soft Matter* **2014**, *10*, 3738−3747.
(48) Haber-Pohlmeier, S.; Abarca-Heidemann, K.; Korschen, H. G.; Dhiman, H. K.; Heberle, J.; Schwalbe, H.; Klein-Seetharaman, J.; Kaupp, U. B.; Pohlmeier, A. Binding of Ca^{2+} to Glutamic Acid-Rich Polypeptides from the Rod Outer Segment. *Biophys. J.* **2007**, *92*, 3207−3214.
(49) Fowler, M.; Siddique, B.; Duhamel, J. Effect of Sequence on the Ionization Behavior of a Series of Amphiphilic Polypeptides. *Langmuir* **2013**, *29*, 4451−4459.
(50) Schaefer, M.; Karplus, M. A Comprehensive Analytical Treatment of Continuum Electrostatics. *J. Phys. Chem.* **1996**, *100*, 1578−1599.
(51) Olsson, M. H. M. Improving the Desolvation Penalty in Empirical Protein pK_a Modeling. *J. Mol. Model.* **2012**, *18*, 1097−1106.
(52) Jacob, M. H.; Amir, D.; Ratner, V.; Gussakowsky, E.; Haas, E. Predicting Reactivities of Protein Surface Cysteines as Part of a Strategy for Selective Multiple Labeling. *Biochemistry* **2005**, *44*, 13664−13672.
(53) Ramachandran, S.; Katha, A. R.; Kolake, S. M.; Jung, B.; Han, S. Dynamics of Dilute Solutions of Poly(Aspartic Acid) and Its Sodium Salt Elucidated from Atomistic Molecular Dynamics Simulations with Explicit Water. *J. Phys. Chem. B* **2013**, *117*, 13906−13913.
(54) Jorgensen, W. L.; Chandrasekhar, J.; Madura, J. D.; Impey, R. W.; Klein, M. L. Comparison of Simple Potential Functions for Simulating Liquid Water. *J. Chem. Phys.* **1983**, *79*, 926−935.
(55) Horn, H. W.; Swope, W. C.; Pitera, J. W.; Madura, J. D.; Dick, T. J.; Hura, G. L.; Head-Gordon, T. Development of an Improved Four-Site Water Model for Biomolecular Simulations: Tip4p-Ew. *J. Chem. Phys.* **2004**, *120*, 9665−9678.
(56) Kusalik, P. G.; Svishchev, I. M. The Spatial Structure in Liquid Water. *Science* **1994**, *265*, 1219−1221.
(57) Kiriukhin, M. Y.; Collins, K. D. Dynamic Hydration Numbers for Biologically Important Ions. *Biophys. Chem.* **2002**, *99*, 155−168.
(58) Collins, K. D. Ions from the Hofmeister Series and Osmolytes: Effects on Proteins in Solution and in the Crystallization Process. *Methods* **2004**, *34*, 300−311.
(59) Collins, K. D.; Neilson, G. W.; Enderby, J. E. Ions in Water: Characterizing the Forces That Control Chemical Processes and Biological Structure. *Biophys. Chem.* **2007**, *128*, 95−104.
(60) Collins, K. D. Why Continuum Electrostatics Theories Cannot Explain Biological Structure, Polyelectrolytes or Ionic Strength Effects in Ion-Protein Interactions. *Biophys. Chem.* **2012**, *167*, 43−59.
(61) Rahman, H. M. A.; Hefter, G.; Buchner, R. Hydration of Formate and Acetate Ions by Dielectric Relaxation Spectroscopy. *J. Phys. Chem. B* **2012**, *116*, 314−323.
(62) Fedotova, M. V.; Kruchinin, S. E. Hydration of Acetic Acid and Acetate Ion in Water Studied by 1D-RISM Theory. *J. Mol. Liq.* **2011**, *164*, 201−206.
(63) Liang, T.; Walsh, T. R. Molecular Dynamics Simulations of Peptide Carboxylate Hydration. *Phys. Chem. Chem. Phys.* **2006**, *8*, 4410−4419.
(64) Grimsley, G. R.; Scholtz, J. M.; Pace, C. N. A Summary of the Measured pK Values of the Ionizable Groups in Folded Proteins. *Protein Sci.* **2009**, *18*, 247−251.
(65) Gallivan, J. P.; Dougherty, D. A. Cation-Π Interactions in Structural Biology. *Proc. Natl. Acad. Sci. U.S.A.* **1999**, *96*, 9459−9464.
(66) Trexler, A. J.; Rhoades, E. N-Terminal Acetylation Is Critical for Forming α-Helical Oligomer of α-Synuclein. *Protein Sci.* **2012**, *21*, 601−605.
(67) Grupi, A.; Haas, E. Segmental Conformational Disorder and Dynamics in the Intrinsically Disordered Protein α-Synuclein and Its Chain Length Dependence. *J. Mol. Biol.* **2011**, *405*, 1267−1283.
(68) Maltsev, A. S.; Ying, J. F.; Bax, A. Impact of N-Terminal Acetylation of Alpha-Synuclein on Its Random Coil and Lipid Binding Properties. *Biochemistry* **2012**, *51*, 5004−5013.
(69) Heyda, J.; Mason, P. E.; Jungwirth, P. Attractive Interactions between Side Chains of Histidine-Histidine and Histidine-Arginine-Based Cationic Dipeptides in Water. *J. Phys. Chem. B* **2010**, *114*, 8744−8749.
(70) Marsili, S.; Chelli, R.; Schettino, V.; Procacci, P. Thermodynamics of Stacking Interactions in Proteins. *Phys. Chem. Chem. Phys.* **2008**, *10*, 2673−2685.
(71) Haghani, K.; Khajeh, K.; Naderi-Manesh, H.; Ranjbar, B. Evidence Regarding the Hypothesis That the Histidine-Histidine Contact Pairs May Affect Protein Stability. *Int. J. Biol. Macromol.* **2012**, *50*, 1040−1047.
(72) Vondrasek, J.; Mason, P. E.; Heyda, J.; Collins, K. D.; Jungwirth, P. The Molecular Origin of Like-Charge Arginine-Arginine Pairing in Water. *J. Phys. Chem. B* **2009**, *113*, 9041−9045.
(73) Humphrey, W.; Dalke, A.; Schulten, K. Vmd: Visual Molecular Dynamics. *J. Mol. Graphics Modell.* **1996**, *14*, 33−38.